https://doi.org/10.5194/egusphere-2026-6690
Preprint. Discussion started: 5 November 2026
© Author(s) 2026. CC BY 4.0 License.

Mechanical controls on the rate of phase transformations in deforming rocks: a numerical study applied to quartz-coesite transformation

Benedek Koszta[1, 2], Kristóf Porkoláb[1], Philippe Yamato[3], Thibault Duretz[4]

[1]HUN-REN Institute of Earth Physics and Space Science, Sopron, Hungary

[2]Eötvös Loránd University, Budapest, Hungary

[3]Univ Rennes, CNRS, UMR 6118, Geosciences Rennes, Rennes, France

[4]Institut für Geowissenschaften, Goethe-Universität Frankfurt, Frankfurt, Germany

Correspondence to: Kristóf Porkoláb (porkolab.kristof@epss.hun-ren.hu)

Abstract. Interactions between deformation and metamorphic transformations influence plate motions, earthquake nucleation and fluid transport and remain a key issue in geodynamics. Here we explore how mechanical parameters (viscosity and strain rate) influence the spatio-temporal evolution of phase transformations in deforming rocks by using numerical models of matrix-clast systems applied to the quartz-coesite transformation example. The amount of transformed material depends on the dynamic pressure magnitude, while in time the transformation shows an exponential evolution toward a steady-state. The magnitude of dynamic pressure depends on the applied deviatoric stress and scales with the Deborah number. However, our parametric study reveals that the transformation (densification) rate is not controlled simply by stress magnitudes, but by the ratio of the deviatoric stress and the characteristic Maxwell time. This means that for a given viscosity distribution, the strain rate controls the densification rate. Our results represent a further step towards predicting the spatio-temporal evolution of the stress field, deformation mechanisms, and mineral phase distributions in natural shear zones or laboratory experiments.

1 Introduction

Deformation and metamorphism in the lithosphere are intrinsically connected (e.g. Brodie and Rutter, 1985). In convergent plate tectonic settings, rocks are tectonically buried, resulting in simultaneous deformation and metamorphic transformation under increasing pressure (P) - temperature (T) conditions. The subduction of tectonic plates produces increasingly denser metamorphic rocks, which influences the dynamics of plate tectonics, the transport of fluids, and deformation mechanisms including the nucleation of earthquakes (Hacker et al., 2003; Hetényi et al., 2007; Malvoisin et al., 2020; Shi et al., 2022; Levitas, 2022; Yamato et al., 2022; Cross et al., 2025; Porkoláb et al., 2025). Hence, the understanding and prediction of spatial and temporal scales of phase transformations constitute key issues in geodynamics. In a deforming medium, pressure

https://doi.org/10.5194/egusphere-2026-6690
Preprint. Discussion started: 5 November 2026
© Author(s) 2026. CC BY 4.0 License.

(or mean stress) can increase through two processes: by burial, which increases the lithostatic loading, and by applied deviatoric stresses, which may locally increase (or decrease) the dynamic pressure component (e.g., Schmid and Podladchikov, 2003; Mancktelow, 2008; Moulas et al., 2014; Yamato and Brun, 2017). Dynamic pressure variations may also lead to metamorphic transformations, as demonstrated by field, laboratory, and numerical studies (Wheeler, 1987; Mancktelow, 1993; Li et al., 2010; Gerya, 2015; Richter et al., 2016; Jamtveit et al., 2018; Luisier et al., 2019; Moulas et al., 2019; Cionoiu et al., 2022; Cochet et al., 2025). Dynamic pressure variations and phase transformations therefore constitute a coupled system, since stress field variations may trigger phase transformations, which in turn affect the deformation pattern and stress field (e.g., Yamato et al., 2022; Baïsset et al., 2024). Therefore, coupled numerical modelling is a key tool to understand phase transformations in deforming rocks.

Numerical modelling studies applying elastic compressibility have already explored various characteristics of coupling between deformation and metamorphic transformations. Yamato et al. (2022) employed pressure overstepping (setting the pressure higher than the pressure of reaction/phase transformation) and showed that the value of overstepping influences the magnitude of shear stress generated by eclogitization. Luisier et al. (2023) imposed dilation/decompression rates to predict fracturing of garnet with coesite inclusions, while Cochet et al. (2025) explored the mechanical conditions of eclogitization in matrix-inclusion systems. In addition to solid-phase compressible models, Malvoisin et al. (2015) and Yarushina et al. (2023) developed the mathematical framework for coupled hydro-mechanical-chemical models. Schmalholz et al. (2020) designed coupled hydro-mechanical-chemical models, using fluid pressure overstepping to induce (de)hydration reactions. Building on this, Schmalholz et al. (2023) and Porkoláb et al. (2025) showed that fluid pressure perturbations that trigger dehydration reactions can also arise from deformation (shear boundary conditions) (Llana-Fúnez et al., 2012). The above-mentioned examples demonstrate that including phase transformations in geodynamic models has high potential in quantifying and predicting the mechanical, structural and geodynamic consequences of coupling between deformation and petrological transformations on tectonic processes.

However, some of the fundamental aspects of coupled numerical models have not been systematically investigated yet. One of these is the time scale of phase transformations in deforming rocks, which is a critical issue for capturing realistic feedback of phase transformations to the stress field and deformation behavior. The study of metamorphic rocks is generally based on equilibrium thermodynamics to describe and model phase transformations/reactions that occur in response to P, T, or composition changes (e.g., Holland and Powell, 1998; Connolly, 2005). Since the concept of equilibrium thermodynamics does not involve a time scale (nor spatial), it is challenging to couple thermodynamics to thermo-mechanical models, where the time scale is critical. In nature, metamorphic transformations do not always take place in true thermodynamic equilibrium and, most of the time, have a time scale. The onset and advance of metamorphic transformations require certain P-T conditions as well as chemical feasibility (availability of required chemical elements and presence of fluids). Reaction kinetics (i.e., the rate of metamorphic transformation) depends on all these aspects: P and T provide the driving force by overstepping equilibrium boundaries, while fluid availability may prohibit or accelerate transformation for a given P-T conditions (Avrami, 1939; Brodie, 1987; Baxter, 2003; Pattison et al., 2011). Polymorphic transformations, such as quartz-

https://doi.org/10.5194/egusphere-2026-6690
Preprint. Discussion started: 5 November 2026
© Author(s) 2026. CC BY 4.0 License.

coesite, may occur instantaneously on geological time scales, with the overall kinetics being controlled by crystal growth processes (Mosenfelder and Bohlen, 1997; Perrillat et al., 2003).

In this study, we focus on pressure-sensitive phase transformations in deforming rocks: pressure increase triggers a prograde phase transformation, assuming that temperature and chemical conditions are sufficient (not rate-limiting). Deformation in rheologically heterogenous rocks gives rise to stress and pressure anomalies (e.g. Moulas et al., 2019). Locally, an increase of dynamic pressure may then lead to reaching the thermodynamic boundary of phase transformations (e.g., Luisier et al., 2023; Cochet et al., 2025). In such cases, dynamic pressure increase rate is a limiting factor for the progress of the phase transformation (rate of density change). As the magnitude of dynamic pressure anomalies and the rate of pressure increase depends on mechanical variables and properties (strain rate, viscosity, compressibility; Moulas et al., 2019), our hypothesis is that the time scale of deformation-induced phase transformations is also controlled by these parameters. Here we test this hypothesis by investigating the temporal and spatial characteristics of solid-phase, deformation-induced phase transformations in simple matrix-inclusion systems, using the quartz-coesite transformation as an example. We use self-developed, two dimensional, Newtonian viscous (but elastically compressible) numerical models to characterize the evolution of the stress field and density in time and space, focusing on dynamic pressure patterns and the intrinsic time scale of the phase transformation. Systematic tests reveal how the above mentioned physical parameters affect dynamic pressure anomalies and the rate of the phase transformation, advancing our knowledge about mechanical controls on transformation rates during prograde metamorphism. These findings can also be used to model natural examples or experimental results of deformation-driven phase transformations and to incorporate phase transformations into more complex geodynamic models.

2. Modelling strategy, setup and validation

Symbol	Meaning	Unit	Value for the reference model
ρ	density	kg·m^{-3}	2763.52 (starting density) at P = 2.76073 GPa and T = 500°C
$\Delta\rho$	density jump	kg·m^{-3}	≈ 208
$\rho_{q,max}$	maximum density of quartz	kg·m^{-3}	2763.53
$\rho_{c,min}$	minimum density of coesite	kg·m^{-3}	2971.32

https://doi.org/10.5194/egusphere-2026-6690
Preprint. Discussion started: 5 November 2026
© Author(s) 2026. CC BY 4.0 License.

β_q	isothermal compressibility of quartz	Pa^{-1}	$\approx 2.3 \cdot 10^{-11}$
β_c	isothermal compressibility of coesite	Pa^{-1}	$\approx 9.38 \cdot 10^{-12}$
P_t	phase transformation pressure	Pa	$2.76873 \cdot 10^{9}$ (phase transformation pressure)
P_d	dynamic pressure	Pa	-
P^{ss}	steady-state pressure	Pa	-
σ_{ij}	stress	Pa	-
τ_{ij}	deviatoric stress	Pa	-
$\dot{\varepsilon}_{ij}$	deviatoric strain rate	s^{-1}	10^{-12} (background)
η	shear viscosity of matrix	Pa·s	$1.2693 \cdot 10^{19}$
η_c	shear viscosity of clast	Pa·s	$0.1 \cdot$
v_i	velocity component	$m \cdot s^{-1}$	-
x_i	spatial coordinates	m	-
δ_{ij}	Kronecker-delta	-	-
t	time	s	-
T	temperature	K	773
$\dot{\rho}$	Densification rate	$kg \cdot m^{-3} \cdot yr^{-1}$	-

Table 1: Symbols used in the mathematical and numerical model description with (SI) units and values for the reference model.

https://doi.org/10.5194/egusphere-2026-6690
Preprint. Discussion started: 5 November 2026
© Author(s) 2026. CC BY 4.0 License.

2.1 Equation solved

We consider an isothermal medium that is Newtonian viscous with respect to shear deformation and elastic with respect to volumetric deformation (compressible). We use the continuity and Stokes equations to solve for the velocity (v) and pressure (p) fields.

The medium is compressible, i.e., density change is included in the continuity equation:

$$\frac{\partial \rho}{\partial t} + \frac{\partial (\rho \cdot v_i)}{\partial x_i} = 0 \tag{1}$$

This conservative form of the continuity equation is often used in a simplified form considering small density variations (e.g., Yamato et al., 2022; Luisier et al., 2023):

$$\frac{\partial \ln \rho}{\partial t} + \frac{\partial v_i}{\partial x_i} = 0 \tag{2}$$

We employ the simplified form Eq. (2) in our model; however, we also tested the fully conservative form Eq. (1), which shows no significant difference for the purpose of our study (see Fig. A1).

By neglecting inertia and gravity and the advection, the momentum equation is expressed as

$$\frac{\partial \sigma_{ij}}{\partial x_j} = 0 \tag{3}$$

where repeated indices imply Einstein summation. The total stress tensor is decomposed into pressure (negative mean stress) and deviatoric stress (τ) components:

$$\sigma_{ij} = -p\delta_{ij} + \tau_{ij} \tag{4}$$

where deviatoric stress is expressed as:

$$\tau_{ij} = 2 \cdot \eta \cdot \dot{\varepsilon}_{ij} \tag{5}$$

$$\dot{\varepsilon}_{ij} = \frac{1}{2} \cdot \left(\frac{\partial v_i}{\partial x_j} + \frac{\partial v_j}{\partial x_i} \right) - \frac{1}{3} \cdot \frac{\partial v_k}{\partial x_k} \delta_{ij} \tag{6}$$

Using Newtonian viscous rheology in our reference model carries the advantage that numerical results can be compared with analytical solutions of the incompressible case (Schmid and Podladchikov, 2003; Moulas et al., 2014) where there is no density variation.

We solve the mathematical model numerically with finite difference discretization (200·200 cells) on a staggered grid, using the accelerated pseudo-transient method (Räss et al., 2022; Alkhimenkov and Podladchikov, 2025), which is commonly used for solving Stokes flow problems in compressible or incompressible systems (e.g., Schmalholz et al., 2020; Halter et al., 2022; Porkoláb et al., 2025;). The self-developed numerical code is available on Zenodo (https://doi.org/10.5281/zenodo.23334817).

https://doi.org/10.5194/egusphere-2026-6690
Preprint. Discussion started: 5 November 2026
© Author(s) 2026. CC BY 4.0 License.

2.1 Model design

As a simple and relevant example, we choose to model the polymorphic quartz-coesite phase transformation. However, our model is also relevant for pressure-sensitive prograde phase transformations/reactions involving a density increase. We set the temperature to 500°C (773 K) and calculate the reference shear viscosity (1.27·1019 Pa·s) via the flow law of dry quartz (Ranalli and Murphy, 1987). We model a matrix-clast system in a 0.1-meter-long square box with a circular weak clast (with one order of magnitude smaller viscosity) located in the center of the model domain (with a 0.005 m radius) (Fig. 1a). Apart from the viscosity, all other properties of the matrix and clast are the same. Viscosity is constant in time and it does not vary due to the phase transformation. We define constant velocities at the edges of the model corresponding to a pure shear boundary condition with a rate of 10^{-12} s^{-1} (Fig. 1a). The initial pressure is homogeneous in the model and is set slightly (8 MPa) below the pressure of the phase transformation. As density is defined by pressure, this means that initially both the matrix and the clast are made of quartz.

Density variation is linked to pressure variation through the compressibility (β). This generally defines a gentle slope in the pressure-density diagram, while a phase transformation defines a sudden jump in density (Fig. 1b). The pressure-density dataset we used for quartz-coesite was computed with PerpleX (Connolly, 2005), using the hp62ver.dat database (Holland and Powell, 1998). We chose not to impose any treatment (smoothing) of this pressure-density data, meaning that the density jump is achieved between two adjacent data points. We also do not implement any kinetic law that would dictate the timing of the phase transformation, in agreement with the instantaneous nucleation outlined by e.g., Perrillat et al. (2003). We update the density based on pressure via linear interpolation between data points, which means that as long as pressure stays between the two „endmember" data points, the density will be „transformational" between $\rho_{q,max}$,$\rho_{c,min}$. (Fig. 1b). Consequently, incremental pressure increase may result in a gradual densification despite the sudden jump in the dataset. We chose this approach because 1) it is the simplest possible case to read pressure-density data exported from a thermodynamic software without imposing reaction kinetics or data smoothing strategies; and 2) this allows us to test the effect of model parameters (e.g., viscosity, strain rate) on the time scale (rate) of phase transformation, simply dictated by the rate of pressure increase.

https://doi.org/10.5194/egusphere-2026-6690
Preprint. Discussion started: 5 November 2026
© Author(s) 2026. CC BY 4.0 License.

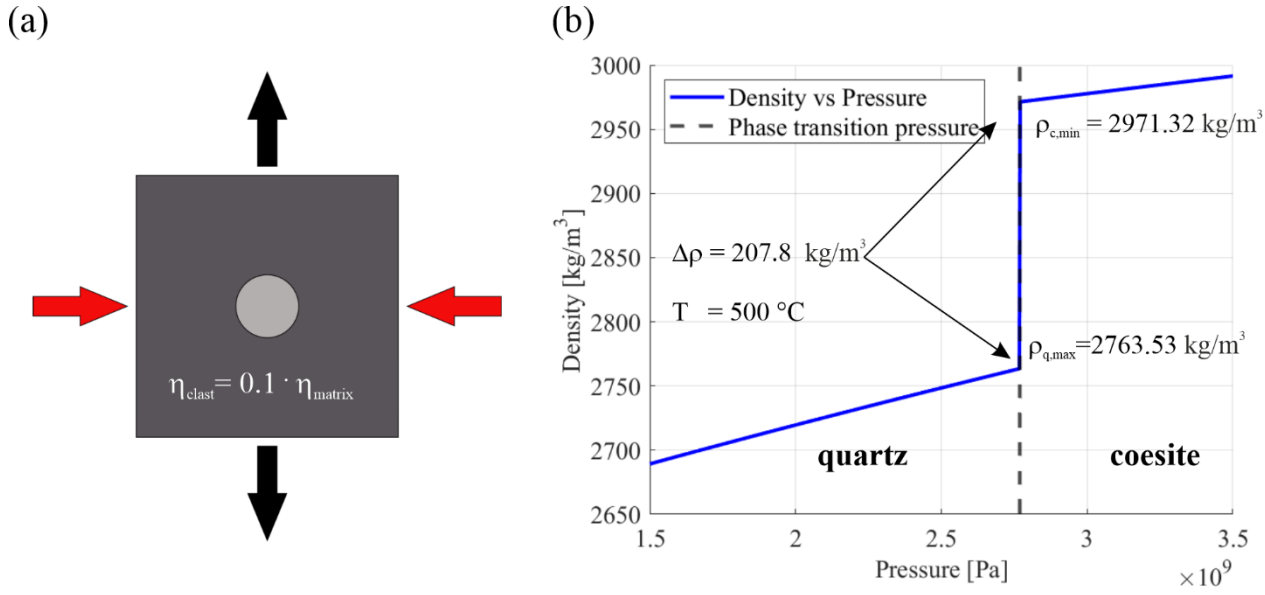


Figure 1: (a): Geometry and boundary conditions of the model. A weak clast (10 times weaker than the matrix) is placed in the centre of the model. The background strain rate is a pure shear boundary condition ($\dot{\varepsilon} = 10^{-12}s^{-1}$) with horizontal shortening (red arrows) and vertical stretching (black arrows). (b): Density-pressure function for the quartz-coesite phase transformation from PerpleX (Connolly, 2005) with the hp62ver.dat database (Holland and Powell, 1998).

2.3. Model validation

We validate our model through comparisons to different solutions (Fig. A2, A3) and via resolution and tolerance tests (Fig. A4). We compare our numerical model with the incompressible analytical solution for elliptical clasts (Schmid and Podladchikov, 2003; Moulas et al., 2014), the incompressible numerical solution, and the compressible numerical solution without phase transformation (Fig. A2). We furthermore test these model variants also for a horizontal layer geometry (Fig. A3, defined in Moulas et al., 2019). Comparisons show that our numerical solution reliably reproduces the pressure fields of the different benchmarks (Fig.s A2, A3). In addition, resolution and pseudo-transient error tolerance tests demonstrate that the reference value for resolution is high enough (N = 200) while the error tolerance is low enough ($\delta = 10^{-4}$) to precisely capture the density evolution (Fig. A4).

To further verify that the simple Newtonian viscous shear rheology of the reference model and the specific form of the continuity equation that we use Eq. (1) do not introduce any artifacts to the density evolution of the model, we compare our reference model to a variant with fully conservative continuity equation, a variant with power-law viscosity, and a variant with Maxwell visco-elastic shear rheology (Fig. A1).

https://doi.org/10.5194/egusphere-2026-6690
Preprint. Discussion started: 5 November 2026
© Author(s) 2026. CC BY 4.0 License.

3. Results

3.1. Model evolution

The pure shear boundary condition induces deformation, which results in dynamic pressure perturbations appearing in the matrix, surrounding the low-viscosity clast, as expected based on analytical and numerical incompressible solutions (Schmid and Podladchikov, 2003; Moulas et al., 2014; Halter et al., 2022). As the setup includes a weak clast, positive dynamic pressure develops on the vertical sides (parallel with σ3), while negative dynamic pressure develops on the horizontal sides (parallel with σ_1) of the clast (Fig. 2a). Pressure at the vertical sides of the clast exceeds the limit of the phase transformation already after the first timestep, triggering the initiation of the quartz-coesite transformation and hence a local density increase. The pressure at this point is between the lower end-member pressure that belongs to quartz ($P_{q,max}$, see Fig. 1b) and the higher end-member pressure that belongs to coesite ($P_{c,min}$). During the phase transformation, pressure is buffered and grows only in small increments (appearing constant on Fig. 2e), slowly approaching the pressure of coesite. Due to the linear interpolation of density based on pressure, density increases gradually in time (between $\rho_{q,max}$ and $\rho_{c,min}$) (Fig. 2f).

We define the duration of phase transformation as the amount of time passed until a given cell reaches the minimum density of coesite ($\rho_{c,min}$) from the maximum density of quartz ($\rho_{q,max}$). Thus, we call a cell „coesite" when the cell reaches $\rho_{c,min}$. When the phase transformation is completed at a given cell, the pressure buffering stops and pressure increases rapidly to reach its steady-state value (Fig. 2e). The amount of coesite (number of completely transformed cells) follows an exponential saturation curve (Fig. 2d). This indicates that the time-dependent system reaches a steady state after some time (all model variants reach steady-state within ~25 kyrs). Consequently, pressure field also reaches a steady state after transformation is completed (Fig. 2a, e), and this steady-state pressure field can be compared to incompressible steady-state solutions (Fig. 3a, A1). As pressure variations are only due to the dynamic component, we use the dynamic pressure as a metric to characterize the model (Fig. 2). We refer to it as P_d and when it reached the steady state, we refer to it as "steady state pressure" (P_d^{ss}).

https://doi.org/10.5194/egusphere-2026-6690
Preprint. Discussion started: 5 November 2026
© Author(s) 2026. CC BY 4.0 License.

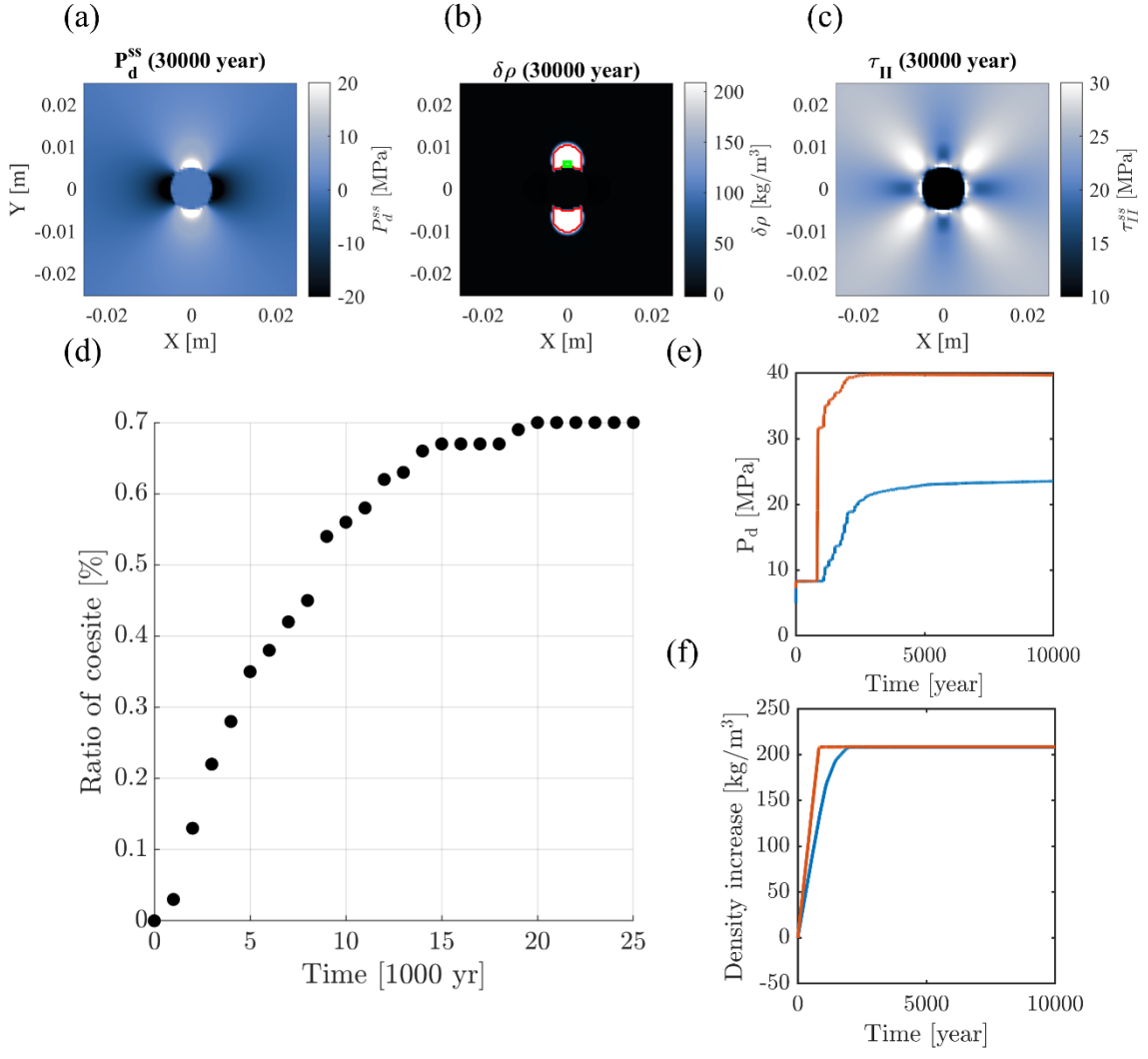


Figure 2: Evolution of the reference model. (a): Close up view of the dynamic pressure field at the center of the reference model after 30,000 years, after the system reached steady state (transformation is completed and dynamic pressure is not increasing anymore). (b): Close up view of the density variation of the model after 30,000 years. The red contour indicates the area of coesite (completely transformed pixels). The green rectangle shows 12 cells that were selected to track pressure and density. These cells transform in every model (in systematic parameter tests) and their average behavior captures the evolution of all different model variants. (c): Close up view of the second invariant of the deviatoric stress tensor after 30,000 years. (d): Proportion of coesite in the reference model over time (ratio of coesite correspond to the ratio of completely transformed cells (i.e. cell only composed by coesite) over the total amount of cells in the model). (e), (f): Dynamic pressure and density variation of the chosen 12 cells (blue, mean value of the 12 cells) and the fastest transforming single cell (red) during the phase transformation. During the phase

https://doi.org/10.5194/egusphere-2026-6690
Preprint. Discussion started: 5 November 2026
© Author(s) 2026. CC BY 4.0 License.

transformation, pressure is buffered and appears constant (increases in very small increments), while density increases linearly in individual cells.

The steady-state pressure field in our model is akin to incompressible solutions (Fig. A2), meaning that pressure is highest close to the low-viscosity clast and gradually decreases towards the edges of the model domain. This pressure field pattern results in a semi-circular area of coesite (Fig. 2a, b). Due to the phase transformation, the steady state pressure in our model shows a consistent deficit compared to the pressure of the incompressible analytical solution (Fig. 3a, A1).

One of the key aspects of our model setup is the intrinsic (non-imposed, arising from mechanical conditions) time scale of the transformation. We characterize this time scale via the transformation or densification rate, defined here as density increase per year. Within a single model, there is a significant spatial variability in the densification rate (see Fig. 3c). Next to the viscosity anomaly (clast), the transformation occurs quite rapidly (high densification rate), while slows down further away from the clast (low densification rate) (Fig. 3c). Plotting the densification rate versus the steady-state pressure for all the transformed cells, we observe a clear correlation: high pressure is coupled with fast transformation (Fig. 3b). In log-log space, faster transforming points fit a line quite well (green line on Fig. 3b). Some outliers are also observed, which are related to the matrix-clast boundary, where numerical errors are highest due to finite difference discretization (Fig. A2). Points where the pressure is barely high enough for transformation to occur, the densification rate tends asymptotically towards zero, therefore not fitting the trend of faster transforming points (Fig. 3b).

https://doi.org/10.5194/egusphere-2026-6690
Preprint. Discussion started: 5 November 2026
© Author(s) 2026. CC BY 4.0 License.

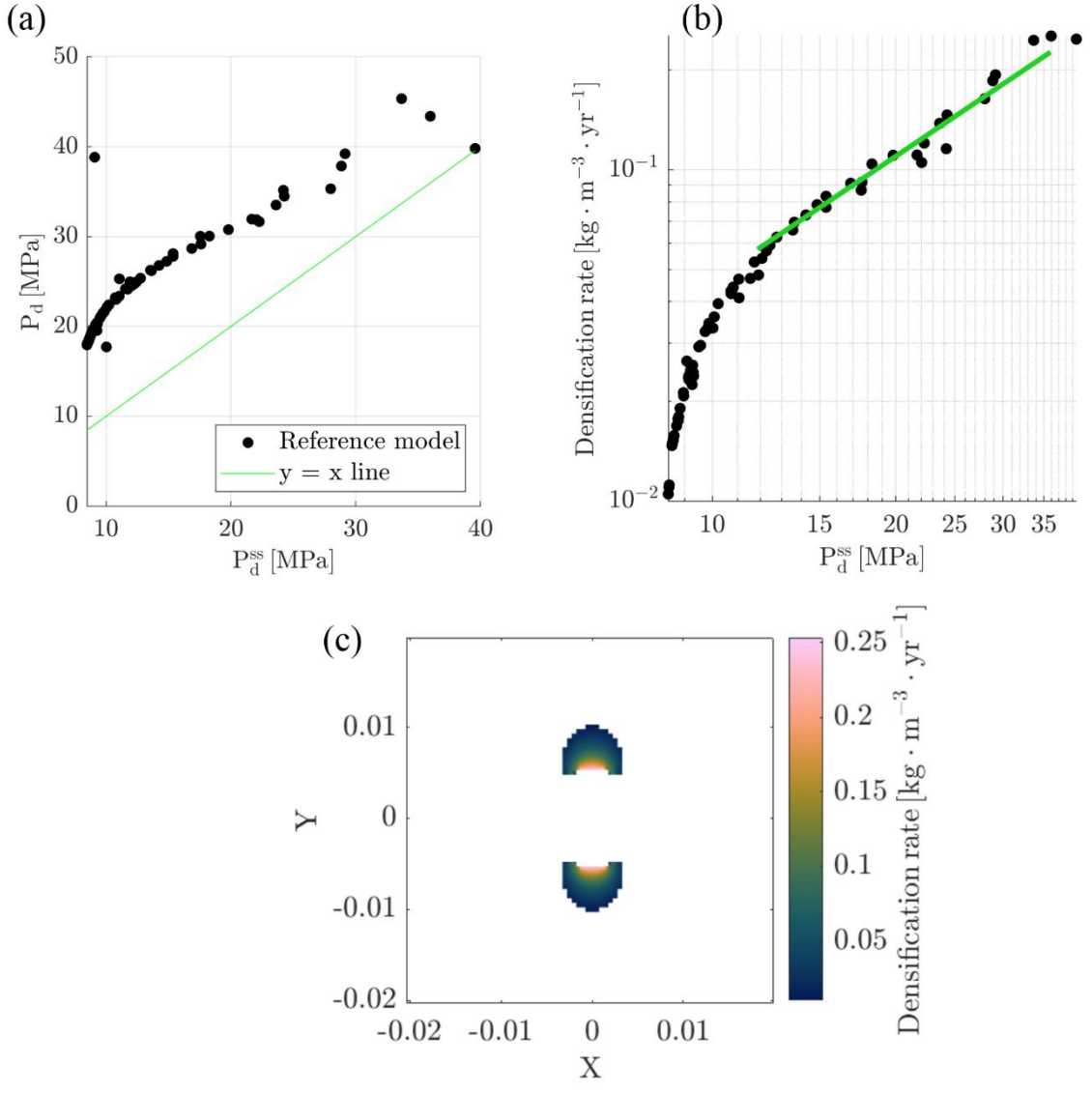


Figure 3: (a): Steady state pressure in the reference model (x-axis) vs the dynamic pressure of the same points in the incompressible analytical solution (P_d) for every transformed cell. Difference from the x=y line shows the effect of including a phase transformation: a consistent pressure deficit of our model with respect to the analytical solution. (b): Steady-state pressure (P_{ss}) vs the densification rate (density increase per year due to phase transformation) for every transformed cell in the reference model on a logarithmic scale (black dots). Green line denotes the linear relation between the P_{ss} and densification rate for the cells where pressure reached at the steady state is high (>12.5 MPa). (c): The spatial distribution of the densification rate in the reference model. Only completely transformed cells are shown.

https://doi.org/10.5194/egusphere-2026-6690
Preprint. Discussion started: 5 November 2026
© Author(s) 2026. CC BY 4.0 License.

3.2. Systematic parameter tests

In natural shear zones, mechanical parameters (e.g., viscosity, strain rate) vary over a wide range, which may affect the progression of phase transformations. We present systematic parameter tests to assess the effects of mechanical parameters (viscosity and applied strain rate) on the model's key characteristics (i.e. pressure reached at the steady state and densification rate).

We varied the imposed background strain rate and the shear viscosity of our reference model to produce 28 different combinations.

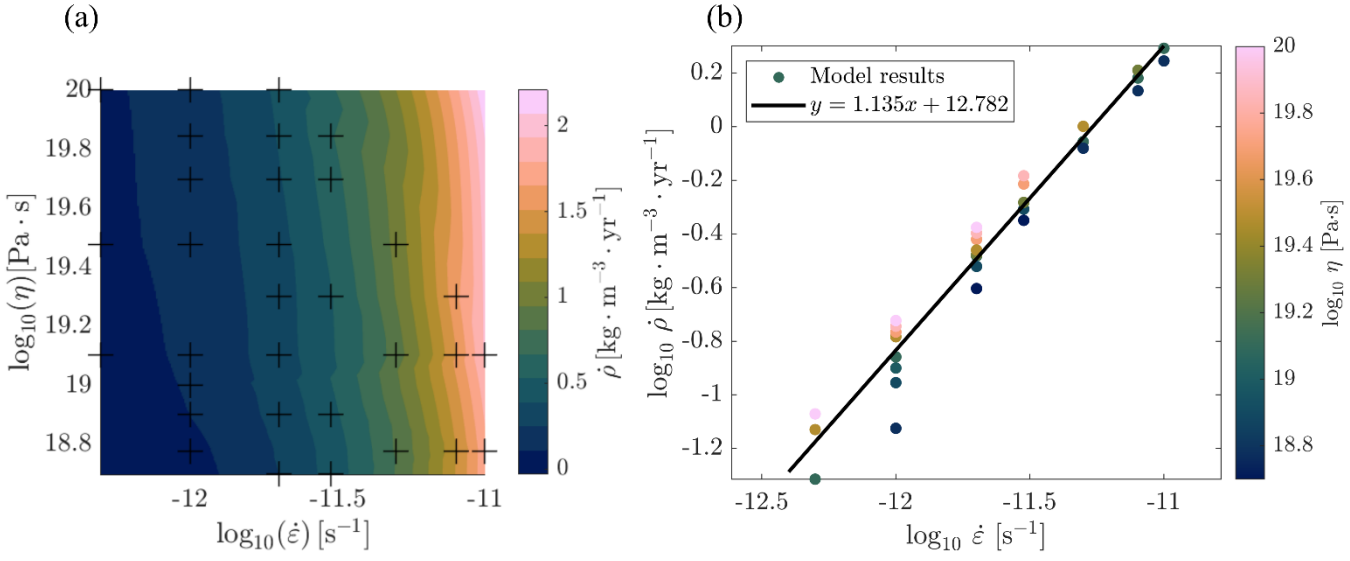


Figure 4: Parametric study on the densification rate ($\dot{\rho}$). (a) Densification rate as a function of viscosity and strain rate. Model results are indicated with black crosses; the colormaps are the product of linear inter- and extrapolation in log-log space. (b) Densification rate ($\dot{\rho}$) as a function of strain rate; fitted line shows their relation in log-log space. Individual model results are plotted as circles and coloured by shear viscosity. Models with smaller viscosity plot under the fitted line, while models with higher viscosity plot above, showing the minor influence of viscosity on $\dot{\rho}$.

The test shows that the densification rate ($\dot{\rho}$) is mostly dependent on the strain rate, while the shear viscosity has minor, almost negligible influence on it (Fig. 4). In other words, the same viscosity may lead to highly variable $\dot{\rho}$, depending on the applied strain rate. This strong strain rate-dependence of $\dot{\rho}$ can be represented by fitting a line in log-log space (Fig. 4b). The minor influence of viscosity (higher viscosity, higher $\dot{\rho}$) is demonstrated by high-viscosity models plotting above the fitted line on Fig. 4b, while low-viscosity models plotting below.

https://doi.org/10.5194/egusphere-2026-6690
Preprint. Discussion started: 5 November 2026
© Author(s) 2026. CC BY 4.0 License.

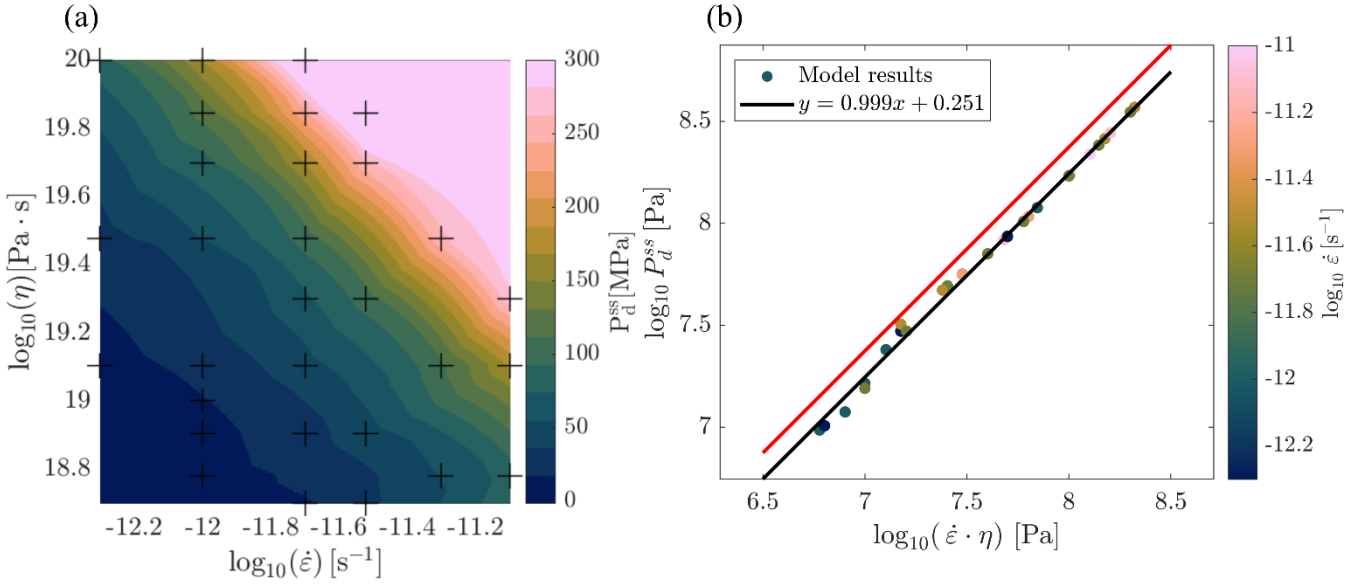


Figure 5: Parametric study on the steady-state pressure. (a) Steady-state pressure as a function of viscosity and strain rate. Model results are indicated with black crosses; the colormaps are the product of linear inter- and extrapolation in log-log space. (b) Steady-state pressure as a function of the product of strain rate and shear viscosity; fitted line shows their relation in log-log space. The red line shows the same relation from the incompressible analytical solution (Schmid and Podlachikov, 2003), showing a consistent pressure deficit. As the difference is constant in logarithmic space, the pressure difference is actually growing with increasing viscosity · strain rate. Individual model results are plotted as circles and coloured by strain rate.

Steady-state pressure (i.e., the dynamic pressure magnitude after the completion of the transformation) shows a different behavior compared to $\dot{\rho}$ as a function of the same variables (Fig. 5). The magnitude of steady-state pressure depends on the strain rate and the shear viscosity equally; the product of these two describes the characteristics of the dynamic pressure perturbation (Fig. 5). Compared to the incompressible analytical solution (Schmid and Podlachikov, 2003), the steady-state pressure in our reference model shows a consistent pressure deficit (Fig. 5b), due to the phase transformation. If the product of viscosity and strain rate is higher, the pressure deficit with respect to the incompressible analytical solution is also higher (Fig. 5b).

4. Discussion

We consider a simplified system where pressure increase triggers a prograde phase transformation, assuming that temperature and chemical conditions are sufficient (not rate-limiting). This simple system has obvious limitations (e.g., not accounting for temperature changes or fluid content) but also the advantage of isolating the investigation of pressure and

https://doi.org/10.5194/egusphere-2026-6690
Preprint. Discussion started: 5 November 2026
© Author(s) 2026. CC BY 4.0 License.

density increase rates in deforming rocks, which is critical in subduction settings. The magnitude of dynamic pressure variations in deforming rocks depends on the strain rate, viscosity (viscosity contrast), and the orientation of the stress field with respect to viscosity heterogeneities (Moulas et al., 2014). In incompressible, viscous models (e.g., Moulas et al., 2014; Halter et al., 2022) the stress (and thus the dynamic pressure) field is instantaneous; it does not involve a time scale. In systems where shear deformation is viscous but volumetric deformation is elastic (such as our reference model), the magnitude of dynamic pressure depends on the same variables; however, stress buildup/relaxation also has a characteristic time scale (Dabrowski et al., 2015; Moulas et al., 2019). This time scale is defined by the characteristic Maxwell-time of the system, in our case given by the ratio of the shear viscosity and the bulk modulus (Moulas et al., 2019).

As pressure increase rates are translated directly to density increase rates in our model, this characteristic time scale is also expected to influence transformation rates. Indeed, our results show that the time scale of dynamic pressure-driven transformation depends on 1) the magnitude of the far-field deviatoric stress ($\tau_{ffs} = 2 \cdot \eta \cdot \dot{\varepsilon}$) that determines dynamic pressure magnitudes (Fig. 5); and 2) the Maxwell-time (t_M) of the system. Systematic analysis reveals that increasing/decreasing both the τ_{ffs} and the t_M by the same amount (thus keeping their ratio, τ_{ffs}/t_M, constant) yields no significant change in $\dot{\rho}$ (Fig. 6a, b). The reason for this behavior is that $\dot{\rho}$ increases with increasing stress and hence dynamic pressure (Fig. 3b) but decreases with increasing t_M, because dynamic pressure buildup and hence transformation is slower for larger t_M (Moulas et al., 2019). This in turn explains the very different effect of strain rate and viscosity on $\dot{\rho}$ (Fig. 4). Viscosity does not affect τ_{ffs}/t_M, as it is a factor in both the numerator and denominator;

$$\frac{\tau_{ffs}}{t_M} = \frac{2 \cdot \eta \cdot \dot{\varepsilon}}{\eta \cdot \beta} = \frac{2 \cdot \dot{\varepsilon}}{\beta} \tag{7}$$

ultimately yielding negligible changes in $\dot{\rho}$ (Fig. 6a, b). In contrast, the imposed boundary strain rate only affects the stress and not the Maxwell time Eq. (7), resulting in strong strain-rate dependence of $\dot{\rho}$ (Fig. 6a, b). The contrasting effects of strain rate and viscosity also explains why τ_{ffs} alone, containing the product of strain rate and viscosity, do not scale with $\dot{\rho}$. The Deborah number ($De = \frac{\text{time of relaxation}}{\text{time of observation}} = \frac{t_M}{\frac{1}{\dot{\varepsilon}}} = \frac{\eta \cdot \beta}{\frac{1}{\dot{\varepsilon}}} = \eta \cdot \beta \cdot \dot{\varepsilon}$; Reiner (1964), used in the sense of Porkoláb et al. (2025)) indicates whether the deformation regime is effectively elastic or effectively viscous and scales with dynamic pressure (Fig. 6c) or fluid pressure magnitudes (Porkoláb et al., 2025) in compressible systems. The *De* is closely related to the far-field stress and consequently shows the same scaling with respect to $\dot{\rho}$: the same *De* may result in highly various $\dot{\rho}$ due to different strain rate/viscosity ratios (Fig. 6a, b). Furthermore, the same holds for mechanical work rate, which also includes the product of viscosity and strain rate ($\dot{W} = \tau \cdot \dot{\varepsilon} = 2 \cdot \eta \cdot \dot{\varepsilon}^2$) in the sense of Baïsset et al., 2024). Overall, our results indicate that the ratio of the far-field deviatoric stress and the Maxwell time exerts significant influence on pressure and density increase rates for dynamic pressure-driven transformations. Practically, for a given viscosity distribution that is defined by lithological variations, τ_{ffs}/t_M (that is in turn controlled by strain rate) is a first-order influence that controls pressure and density increase rates in tectonic overpressure zones.

https://doi.org/10.5194/egusphere-2026-6690
Preprint. Discussion started: 5 November 2026
© Author(s) 2026. CC BY 4.0 License.

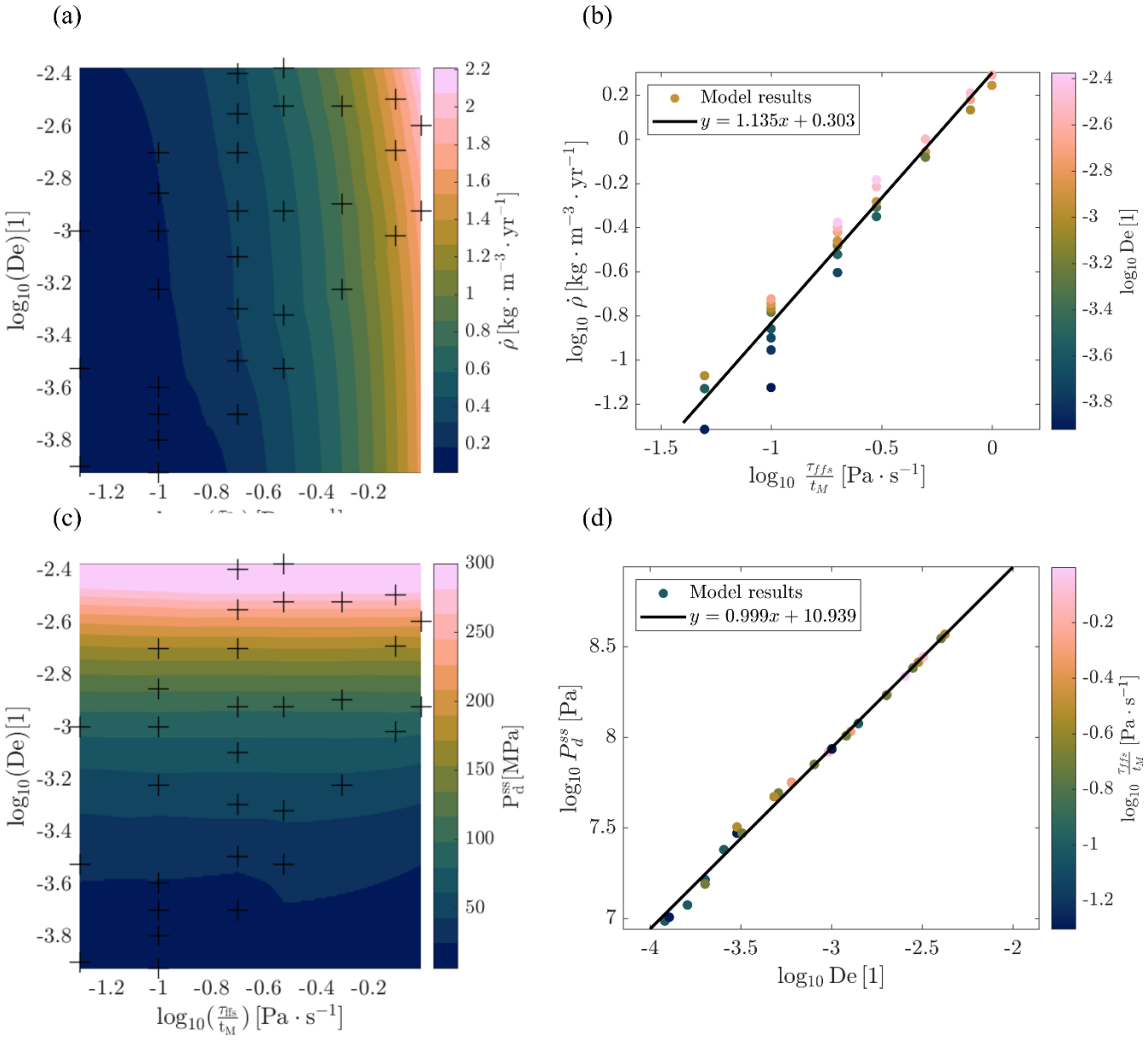


Figure 6: Systematic analysis of the densification rate ($\dot{\rho}$) and the steady-state pressure (P_d^{ss}). (a) $\dot{\rho}$ as a function of the far-field deviatoric stress/Maxwell-time ratio (τ_{ffs}/t_M) and the Deborah number (De). Model results are indicated with black crosses; the colormaps are the product of linear inter- and extrapolation in log-log space. (b) $\dot{\rho}$ as a function of τ_{ffs}/t_M; fitted line shows their relation in log-log space. Individual model results are plotted as circles and coloured by the De, showing its minor influence on $\dot{\rho}$. (c) P_d^{ss} as a function τ_{ffs}/t_M De. (d) P_d^{ss} as a function of De; fitted line shows their relation in log-log space. Individual model results are plotted as circles and coloured by τ_{ffs}/t_M, showing its negligible influence on P_d^{ss}.

https://doi.org/10.5194/egusphere-2026-6690
Preprint. Discussion started: 5 November 2026
© Author(s) 2026. CC BY 4.0 License.

These findings are relevant for the design of models where feedback between deformation and phase transformations is important. Understanding the evolution of natural shear zones in geodynamic models or laboratory experiments (and their extrapolation to natural conditions) requires predictive models both in time and space. Supplemented with realistic shear zone geometries, shearing rates and viscosity distributions, our model could be used to study natural cases of phase transformations in tectonic overpressure zones (e.g., Mancktelow, 1993; Jamtveit et al., 2018; Luisier et al., 2019). In addition, including transformation kinetics (accounting for temperature, chemical conditions, fluid content) would superimpose another time scale on top of the inherent time scale of pressure and density change rates that are controlled by mechanical properties. In this case, the mechanical limits (controlled by τ_{ffs}/t_M for a given viscosity contrast) would provide a maximum transformation rate, which could potentially be decelerated by kinetic conditions.

Another key goal of numerical models is to predict the spatial patterns of phase transformation-deformation interactions, which require realistic pressure field predictions. Our systematic analysis shows that steady-state pressure magnitude is predicted by the *De* (or the deviatoric stress magnitude), while in contrast to densification rates, steady-state pressure magnitude is not sensitive to changes in the τ_{ffs}/t_M (Fig. 6c, d). Results show furthermore that the different types of incompressible and compressible matrix-clast system models yield a similar pressure and stress field pattern around the viscosity anomalies (Fig. A2). This allows the first-order numerical determination of dynamic pressure patterns also in more complex shear zones or laboratory experiments (e.g., using incompressible models such as Cionoiu et al., 2022). We furthermore show that due to the densification, the post-transformation steady-state pressure is consistently lower than in the other solutions (Fig.s 3b, A1), which means that our model may be used for refined predictions compared to models without phase transformations (e.g., Cionoiu et al., 2022).

Regarding pressure and transformation patterns, we note that in our model, shear viscosity stays constant throughout the quartz-coesite transformation, which could indeed be close to reality based on Hunt et al. (2019), but nevertheless remains uncertain. If viscosity was variable (quartz and coesite having significantly different viscosities), the direction of overpressure and transformation propagation would depend on the relative viscosity of the reaction/transformation product and the orientation of the stress field (imposed shortening and extension directions). For high-viscosity transformation products, overpressure and hence transformation is expected to propagate parallel with the shortening direction (Moulas et al., 2014). In case of weaker reaction/transformation products, the central low-viscosity anomaly in the model grows normal to the shortening direction, prolonging the overpressure/transformation area and eventually producing finger-like structures (e.g., Cochet et al., 2025; Porkoláb et al., 2025).

5. Conclusion

We aimed to explore how mechanical parameters influence the spatio-temporal evolution of phase transformations in deforming rocks by 2D, finite difference, numerical models of matrix-clast systems, using the quartz-coesite transformation as an example. Pure shear boundary conditions induce dynamic pressure variations around a weak (low-viscosity) clast

https://doi.org/10.5194/egusphere-2026-6690
Preprint. Discussion started: 5 November 2026
© Author(s) 2026. CC BY 4.0 License.

embedded in a stronger matrix. The phase transformation is triggered once the pressure reaches the transformation pressure, while density is updated based on pressure. The amount of transformed material depends on the dynamic pressure magnitude, while in time, the transformation shows an exponential saturation, meaning that steady-state is reached eventually. The magnitude of dynamic pressure depends on the deviatoric stress and hence also scales with the Deborah number. In contrast, our results reveal that the transformation rate is not controlled simply by stress magnitudes, but also by the ratio of the deviatoric stress and the Maxwell-time, which in turn is controlled by the imposed strain rate. These results contribute to our understanding of interactions between mechanics and metamorphic transformations and represent a further step towards predicting the spatio-temporal evolution of the stress field, deformation mechanisms, and mineral phase distributions in natural shear zones or laboratory experiments.

Appendix A

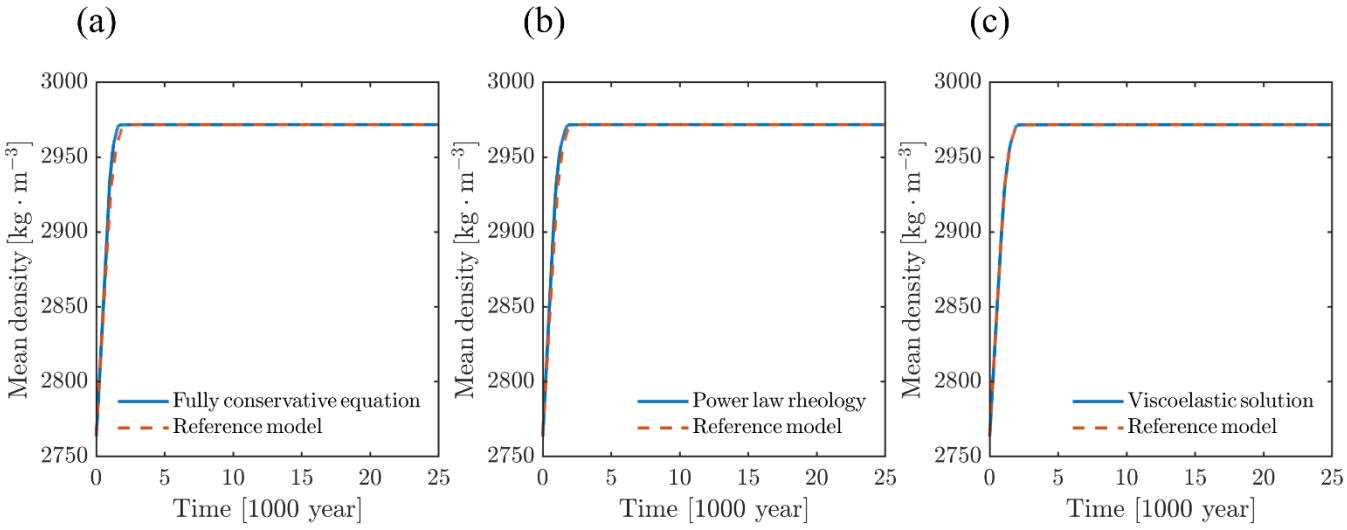
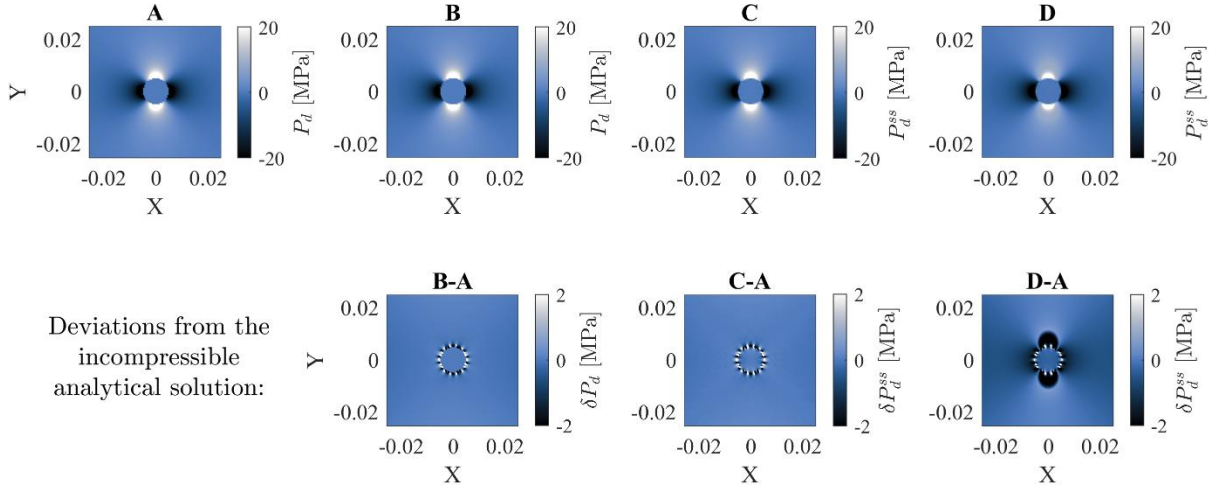


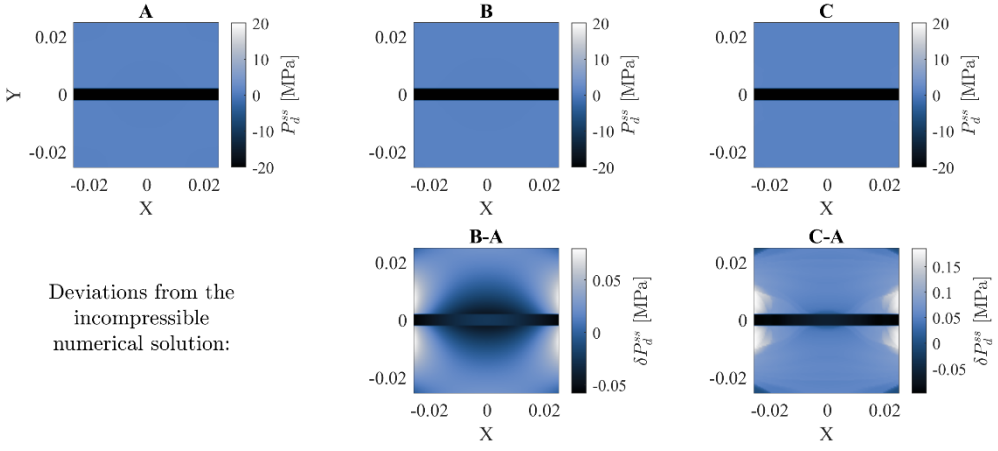
Figure A1: Comparison of our modelling strategy to different solutions. (a) The comparison with the fully conservative continuity equation ($\frac{\partial \rho}{\partial t} + \frac{\partial(\rho \cdot v_i)}{\partial x_j} = 0$). The average density of the investigated 12 cells shows that the used equations are accurate enough for the problem. (b) The comparison of the reference model (Newtonian viscous rheology) with power law viscosity (n =2.4) (Brace and Kohlstedt, 1980) and (c) viscoelastic rheology (Maxwell model). It shows that Newtonian viscous rheology results in the same characteristics. In both panels, the average density of the investigated 12 cells is shown.

https://doi.org/10.5194/egusphere-2026-6690
Preprint. Discussion started: 5 November 2026
© Author(s) 2026. CC BY 4.0 License.



340

Figure A2: The comparison of the different modelling strategies for the deformation of matrix-clast systems. Parameters matching the reference model were used in all other models. A: Dynamic pressure field of the incompressible analytical solution (Schmid and Podladchikov, 2003). B: The dynamic pressure field of the incompressible numerical solution. C: The steady state dynamic pressure field of the compressible numerical model 345 **without phase transformation. In this case, the density varies only because of compressibility, but every parameter is the same as the reference model. D: The steady state dynamic pressure field of the compressible numerical solution with phase transformation (reference model). Lower row: The deviation of all the models from the incompressible analytical solution. In all numerical models, there is a ≈10% numerical error at the viscosity contrast due to finite difference discretization, which is a localized and well-described phenomenon (Deubelbeiss and Kaus, 2008). The** 350 **models show that only the density jump of the phase transformation causes significant pressure deviation from the incompressible analytical solution.**



https://doi.org/10.5194/egusphere-2026-6690
Preprint. Discussion started: 5 November 2026
© Author(s) 2026. CC BY 4.0 License.

Figure A3: The comparison of the different modelling techniques for a weak layer (like the strong layer benchmark of Moulas et al. (2019)). The viscosity of the layer is the tenth of the matrix, similar to the reference model. In the upper row the dynamic pressures, in the lower row the pressure deviations from the incompressible numerical solution are shown. A: The incompressible numerical solution of the weak layer model. B: The compressible numerical solution of the weak layer model. C: The compressible numerical model with phase transformation for the weak layer model. Lower row: The deviation from the incompressible numerical solution.

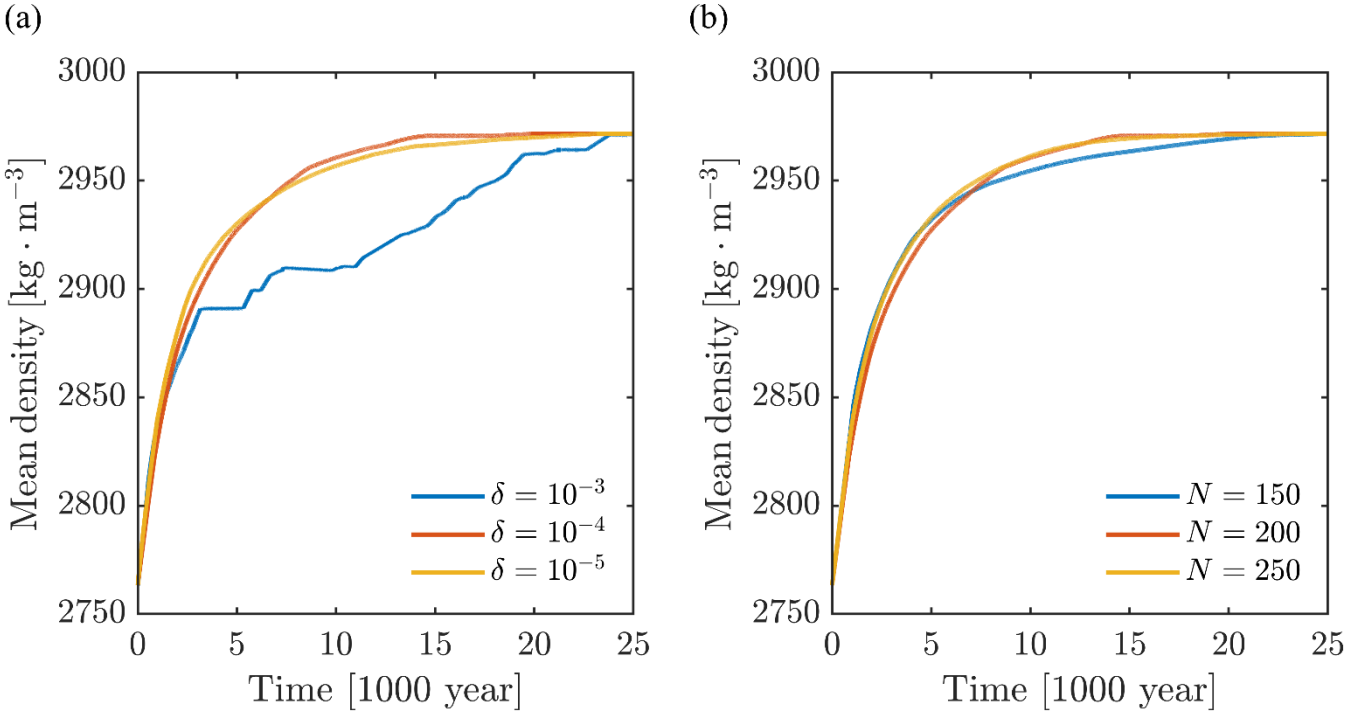


Figure A4: Tolerance and resolution test. (a) The mean pressure of the transformed cells for different tolerance values (δ) used for the convergence of the pseudo-transient method. (b) The mean pressure of the transformed cells for different resolutions (N corresponds to the number of vertices). These tests show that the used numerical parameters ($N = 200$, $\delta = 10^{-4}$) are accurate enough.

Code availability

All results have been generated with a self-developed MATLAB code, which is available on the platform Zenodo: https://doi.org/10.5281/zenodo.23334817.

https://doi.org/10.5194/egusphere-2026-6690
Preprint. Discussion started: 5 November 2026
© Author(s) 2026. CC BY 4.0 License.

Author contributions

B.K.: Formal analysis, Investigation, Methodology, Software, Validation, Visualization, Writing (original draft preparation). **K.P.**: Conceptualization, Investigation, Methodology, Software, Supervision, Writing (original draft preparation), Writing (review and editing). **P.Y.**: Conceptualization, Writing (review and editing). **T.D.**: Conceptualization, Writing (review and editing).

Competing interests

The authors declare that they have no known competing financial interests or personal relationships that could have appeared to influence the work reported in this paper.

Disclaimer

Copernicus Publications remains neutral with regard to jurisdictional claims made in the text, published maps, institutional affiliations, or any other geographical representation in this paper. While Copernicus Publications makes every effort to include appropriate place names, the final responsibility lies with the authors. Views expressed in the text are those of the authors and do not necessarily reflect the views of the publisher.

Acknowledgements

The authors thank Evangelos Moulas, Stefan Schmalholz, and Attila Galsa for stimulating discussions that helped to shape the study.

Financial support

B.K. was supported by the EKÖP-26 university research scholarship program of the Ministry of Science and Technology from the source of the National Research, Development and Innovation Fund. K.P. was supported by the János Bolyai Research Scholarship of the Hungarian Academy of Sciences and by the MTA FI FluidsByDepth Lendület (Momentum) project provided by the Hungarian Academy of Sciences (LP2022-2/2022). P.Y. also acknowledges the ANR for its support of the METROLOGY project (ANR-23-CE49-0008), which investigates the links between metamorphic transformations and rock deformation, and the Heraeus Foundation for supporting his visiting professorship at the Institute of Geosciences, Goethe University Frankfurt.

https://doi.org/10.5194/egusphere-2026-6690
Preprint. Discussion started: 5 November 2026
© Author(s) 2026. CC BY 4.0 License.

References

Alkhimenkov, Y., Podladchikov, Y.Y., 2025. Accelerated pseudo-transient method for elastic, viscoelastic, and coupled hydromechanical problems with applications. Geosci. Model Dev. 18, 563–583. https://doi.org/10.5194/gmd-18-563-2025

Avrami, M., 1939. Kinetics of Phase Change. I General Theory. J. Chem. Phys. 7, 1103–1112. https://doi.org/10.1063/1.1750380

Baïsset, M., Yamato, P., Duretz, T., 2024. Weakening Induced by Phase Nucleation in Metamorphic Rocks: Insights From Numerical Models. Geochem. Geophys. Geosystems 25, e2024GC011706. https://doi.org/10.1029/2024GC011706

Baxter, E.F., 2003. Natural constraints on metamorphic reaction rates. Geol. Soc. Lond. Spec. Publ. 220, 183–202. https://doi.org/10.1144/GSL.SP.2003.220.01.11

Brace, W.F., Kohlstedt, D.L., 1980. Limits on lithospheric stress imposed by laboratory experiments. J. Geophys. Res. Solid Earth 85, 6248–6252. https://doi.org/10.1029/JB085iB11p06248

Brodie, K., 1987. Metamorphic studies: research in progress. J. Geol. Soc. 144, 519–522. https://doi.org/10.1144/gsjgs.144.3.0519

Brodie, K.H., Rutter, E.H., 1985. On the Relationship between Deformation and Metamorphism, with Special Reference to the Behavior of Basic Rocks, in: Thompson, A.B., Rubie, D.C. (Eds.), Metamorphic Reactions, Advances in Physical Geochemistry. Springer New York, New York, NY, pp. 138–179. https://doi.org/10.1007/978-1-4612-5066-1_6

Cionoiu, S., Moulas, E., Stünitz, H., Tajčmanová, L., 2022. Locally Resolved Stress-State in Samples During Experimental Deformation: Insights Into the Effect of Stress on Mineral Reactions. J. Geophys. Res. Solid Earth 127, e2022JB024814. https://doi.org/10.1029/2022JB024814

Cochet, A., Yamato, P., Baïsset, M., Duretz, T., Labrousse, L., 2025. What Controls Finger-Shaped Transformation Patterns? A Numerical Approach to Eclogitization. Geochem. Geophys. Geosystems 26, e2025GC012457. https://doi.org/10.1029/2025GC012457

Connolly, J.A.D., 2005. Computation of phase equilibria by linear programming: A tool for geodynamic modeling and its application to subduction zone decarbonation. Earth Planet. Sci. Lett. 236, 524–541. https://doi.org/10.1016/j.epsl.2005.04.033

Crameri, F., 2018. Geodynamic diagnostics, scientific visualisation and StagLab 3.0. Geosci. Model Dev. 11, 2541–2562. https://doi.org/10.5194/gmd-11-2541-2018

Cross, A.J., Goddard, R.M., Kumamoto, K.M., Goldsby, D.L., Hansen, L.N., Chen, H., Hein, D., Thom, C.A., Nehring, M.A., Breithaupt, T., Wallis, D., 2025. Direct observations of transient weakening during phase transformations in quartz and olivine. Nat. Geosci. 18, 548–554. https://doi.org/10.1038/A41561-025-01703-6

Dabrowski, M., Powell, R., Podladchikov, Y., 2015. Viscous relaxation of grain-scale pressure variations. J. Metamorph. Geol. 33, 859–868. https://doi.org/10.1111/jmg.12142

https://doi.org/10.5194/egusphere-2026-6690
Preprint. Discussion started: 5 November 2026
© Author(s) 2026. CC BY 4.0 License.

Deubelbeiss, Y., Kaus, B.J.P., 2008. Comparison of Eulerian and Lagrangian numerical techniques for the Stokes equations in the presence of strongly varying viscosity. Phys. Earth Planet. Inter. 171, 92–111. https://doi.org/10.1016/j.pepi.2008.06.023

Gerya, T., 2015. Tectonic overpressure and underpressure in lithospheric tectonics and metamorphism. J. Metamorph. Geol. 33, 785–800. https://doi.org/10.1111/jmg.12144

Hacker, B.R., Peacock, S.M., Abers, G.A., Holloway, S.D., 2003. Subduction factory 2. Are intermediate-depth earthquakes in subducting slabs linked to metamorphic dehydration reactions? J. Geophys. Res. Solid Earth 108, 2001JB001129. https://doi.org/10.1029/2001JB001129

Halter, W.R., Macherel, E., Schmalholz, S.M., 2022. A simple computer program for calculating stress and strain rate in 2D viscous inclusion-matrix systems. J. Struct. Geol. 160, 104617. https://doi.org/10.1016/j.jsg.2022.104617

Hetényi, G., Cattin, R., Brunet, F., Bollinger, L., Vergne, J., Nábělek, J.L., Diament, M., 2007. Density distribution of the India plate beneath the Tibetan plateau: Geophysical and petrological constraints on the kinetics of lower-crustal eclogitization. Earth Planet. Sci. Lett. 264, 226–244. https://doi.org/10.1016/j.epsl.2007.09.036

Holland, T.J.B., Powell, R., 1998. An internally consistent thermodynamic data set for phases of petrological interest. J. Metamorph. Geol. 16, 309–343. https://doi.org/10.1111/j.1525-1314.1998.00140.x

Hunt, S.A., Whitaker, M.L., Bailey, E., Mariani, E., Stan, C.V., Dobson, D.P., 2019. An Experimental Investigation of the Relative Strength of the Silica Polymorphs Quartz, Coesite, and Stishovite. Geochem. Geophys. Geosystems 20, 1975–1989. https://doi.org/10.1029/2018GC007842

Jamtveit, B., Moulas, E., Andersen, T.B., Austrheim, H., Corfu, F., Petley-Ragan, A., Schmalholz, S.M., 2018. High Pressure Metamorphism Caused by Fluid Induced Weakening of Deep Continental Crust. Sci. Rep. 8, 17011. https://doi.org/10.1038/A41598-018-35200-1

Levitas, V.I., 2022. Resolving puzzles of the phase-transformation-based mechanism of the strong deep-focus earthquake. Nat. Commun. 13, 6291. https://doi.org/10.1038/A41467-022-33802-y

Li, Z.H., Gerya, T.V., Burg, J. -P., 2010. Influence of tectonic overpressure on P–T paths of HP–UHP rocks in continental collision zones: thermomechanical modelling. J. Metamorph. Geol. 28, 227–247. https://doi.org/10.1111/j.1525-1314.2009.00864.x

Llana-Fúnez, S., Wheeler, J., Faulkner, D.R., 2012. Metamorphic reaction rate controlled by fluid pressure not confining pressure: implications of dehydration experiments with gypsum. Contrib. Mineral. Petrol. 164, 69–79. https://doi.org/10.1007/s00410-012-0726-8

Luisier, C., Baumgartner, L., Schmalholz, S.M., Siron, G., Vennemann, T., 2019. Metamorphic pressure variation in a coherent Alpine nappe challenges lithostatic pressure paradigm. Nat. Commun. 10, 4734. https://doi.org/10.1038/A41467-019-12727-z

Luisier, C., Tajčmanová, L., Yamato, P., Duretz, T., 2023. Garnet microstructures suggest ultra-fast decompression of ultrahigh-pressure rocks. Nat. Commun. 14, 6012. https://doi.org/10.1038/A41467-023-41310-w

https://doi.org/10.5194/egusphere-2026-6690
Preprint. Discussion started: 5 November 2026
© Author(s) 2026. CC BY 4.0 License.

Malvoisin, B., Austrheim, H., Hetényi, G., Reynes, J., Hermann, J., Baumgartner, L.P., Podladchikov, Y.Y., 2020. Sustainable densification of the deep crust. Geology 48, 673–677. https://doi.org/10.1130/G47201.1

Malvoisin, B., Podladchikov, Y.Yu., Vrijmoed, J.C., 2015. Coupling changes in densities and porosity to fluid pressure variations in reactive porous fluid flow: Local thermodynamic equilibrium. Geochem. Geophys. Geosystems 16, 4362–4387. https://doi.org/10.1002/2015GC006019

Mancktelow, N.S., 2008. Tectonic pressure: Theoretical concepts and modelled examples. Lithos 103, 149–177. https://doi.org/10.1016/j.lithos.2007.09.013

Mancktelow, N.S., 1993. Tectonic overpressure in competent mafic layers and the development of isolated eclogites. J. Metamorph. Geol. 11, 801–812. https://doi.org/10.1111/j.1525-1314.1993.tb00190.x

Mosenfelder, J.L., Bohlen, S.R., 1997. Kinetics of the coesite to quartz transformation. Earth Planet. Sci. Lett. 153, 133–147. https://doi.org/10.1016/S0012-821X(97)00159-3

Moulas, E., Burg, J.-P., Podladchikov, Y., 2014. Stress field associated with elliptical inclusions in a deforming matrix: Mathematical model and implications for tectonic overpressure in the lithosphere. Tectonophysics 631, 37–49. https://doi.org/10.1016/j.tecto.2014.05.004

Moulas, E., Schmalholz, S.M., Podladchikov, Y., Tajčmanová, L., Kostopoulos, D., Baumgartner, L., 2019. Relation between mean stress, thermodynamic, and lithostatic pressure. J. Metamorph. Geol. 37, 1–14. https://doi.org/10.1111/jmg.12446

Pattison, D.R.M., De Capitani, C., Gaidies, F., 2011. Petrological consequences of variations in metamorphic reaction affinity: PETROLOGICAL CONSEQUENCES OF VARIATIONS IN METAMORPHIC REACTION AFFINITY. J. Metamorph. Geol. 29, 953–977. https://doi.org/10.1111/j.1525-1314.2011.00950.x

Perrillat, J.P., Daniel, I., Lardeaux, J.M., Cardon, H., 2003. Kinetics of the Coesite-Quartz Transformation: Application to the Exhumation of Ultrahigh-Pressure Rocks. J. Petrol. 44, 773–788. https://doi.org/10.1093/petrology/44.4.773

Porkoláb, K., Moulas, E., Schmalholz, S.M., 2025. Modeling the Interplay Between Reaction Progress, Deformation and Stress Field Evolution During Antigorite Dehydration: Implications for Intermediate-Depth Seismicity. Geophys. Res. Lett. 52, e2024GL113865. https://doi.org/10.1029/2024GL113865

Ranalli, G., Murphy, D.C., 1987. Rheological stratification of the lithosphere. Tectonophysics 132, 281–295. https://doi.org/10.1016/0040-1951(87)90348-9

Räss, L., Utkin, I., Duretz, T., Omlin, S., Podladchikov, Y.Y., 2022. Assessing the robustness and scalability of the accelerated pseudo-transient method. Geosci. Model Dev. 15, 5757–5786. https://doi.org/10.5194/gmd-15-5757-2022

Reiner, M., 1964. The Deborah Number. Phys. Today 17, 62–62. https://doi.org/10.1063/1.3051374

Richter, B., Stünitz, H., Heilbronner, R., 2016. Stresses and pressures at the quartz-to-coesite phase transformation in shear deformation experiments. J. Geophys. Res. Solid Earth 121, 8015–8033. https://doi.org/10.1002/2016JB013084

https://doi.org/10.5194/egusphere-2026-6690
Preprint. Discussion started: 5 November 2026
© Author(s) 2026. CC BY 4.0 License.



Schmalholz, S.M., Moulas, E., Plümper, O., Myasnikov, A.V., Podladchikov, Y.Y., 2020. 2D Hydro-Mechanical-Chemical Modeling of (De)hydration Reactions in Deforming Heterogeneous Rock: The Periclase-Brucite Model Reaction. Geochem. Geophys. Geosystems 21, e2020GC009351. https://doi.org/10.1029/2020GC009351

Schmalholz, S.M., Moulas, E., Räss, L., Müntener, O., 2023. Serpentinite Dehydration and Olivine Vein Formation During Ductile Shearing: Insights From 2D Numerical Modeling on Porosity Generation, Density Variations, and Transient Weakening. J. Geophys. Res. Solid Earth 128, e2023JB026985. https://doi.org/10.1029/2023JB026985

Schmid, D.W., Podladchikov, Y.Yu., 2003. Analytical solutions for deformable elliptical inclusions in general shear. Geophys. J. Int. 155, 269–288. https://doi.org/10.1046/j.1365-246X.2003.02042.x

Shi, F., Wang, Y., Wen, J., Yu, T., Zhu, L., Huang, T., Wang, K., 2022. Metamorphism-facilitated faulting in deforming orthopyroxene: Implications for global intermediate-depth seismicity. Proc. Natl. Acad. Sci. 119, e2112386119. https://doi.org/10.1073/pnas.2112386119

Wheeler, J., 1987. The significance of grain-scale stresses in the kinetics of metamorphism. Contrib. Mineral. Petrol. 97, 397–404. https://doi.org/10.1007/BF00372002

Yamato, P., Brun, J.P., 2017. Metamorphic record of catastrophic pressure drops in subduction zones. Nat. Geosci. 10, 46–50. https://doi.org/10.1038/ngeo2852

Yamato, P., Duretz, T., Baïsset, M., Luisier, C., 2022. Reaction-induced volume change triggers brittle failure at eclogite facies conditions. Earth Planet. Sci. Lett. 584, 117520. https://doi.org/10.1016/j.epsl.2022.117520

Yarushina, V.M., Podladchikov, Y.Y., Wang, H., 2023. On the Constitutive Equations for Coupled Flow, Chemical Reaction, and Deformation of Porous Media. J. Geophys. Res. Solid Earth 128, e2023JB027725. https://doi.org/10.1029/2023JB027725